eJSSNT Technical Note

e-Journal of Surface Science and Nanotechnology **22**, 170–173 (2024)

Time-of-Flight-type Photoelectron Emission Microscopy with a 10.9-eV Laser

Shunsuke Tsuda,† Koichiro Yaji

Center for Basic Research on Materials, National Institute for Materials Science, 3-13 Sakura, Tsukuba, Ibaraki 305-0003, Japan
† *Corresponding author: TSUDA.Shunsuke@nims.go.jp*

Received: 22 November, 2023; Accepted: 31 December, 2023; J-STAGE Advance Publication: 17 February, 2024; Published: 17 February, 2024

We have developed a novel photoemission microscopy apparatus employing a vacuum ultraviolet laser. This setup combines photoemission electron microscopy (PEEM) with a time-of-flight detector, facilitating rapid visualization of electronic states in both real and momentum space. Achieving a spatial resolution of 70 nm, attributed to the PEEM lens system, we showcase the full band mapping of a Bi(111) single crystal film using angle-resolved photoemission spectroscopy within a short acquisition time.

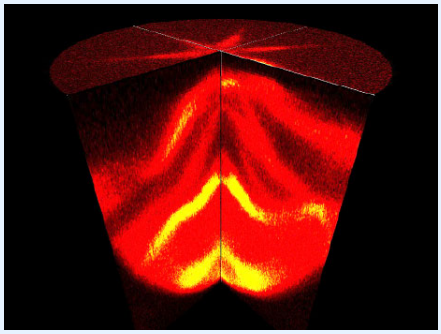

Keywords *Photoemission spectroscopy; Momentum microscope; Ultraviolet laser; Electronic property; Time of flight*

I. INTRODUCTION

Photoelectron spectroscopy provides direct insights into the electronic states of materials by measuring the kinetic energy of photoelectrons emitted upon irradiation with light exceeding the work function and emission frequency at that energy [1]. In the context of single-crystalline samples, the emission angle furnishes information on the momentum of electrons in the material, giving rise to angle-resolved photoemission spectroscopy (ARPES), a technique that has significantly advanced condensed matter physics.

The advancement of ARPES technology parallels enhancements in hemispherical photoelectron analyzers, evolving rapidly over the last quarter century to achieve exceptional energy resolution [2]. Hemispherical energy analyzers, capable of directly visualizing the band structure, prove especially well-suited for investigating electronic properties and solid-state physics. However, their inherent limitation lies in measuring only a specific narrow energy range simultaneously, discarding information from other photoelectrons and presenting challenges for samples with weak photoelectron signals. Conversely, the time-of-flight (ToF) analyzer, a detector for photoemission spectroscopy with a 50-year history [3], detects differences in kinetic energy by measuring the time it takes for photoelectrons to reach the detector. While highly efficient as it captures all electrons, ToF analyzers necessitate a pulsed light source and have predominantly been used with synchrotron radiation.

In laboratory systems, pulsed-laser lights are employed for photoelectron spectroscopy with ToF detectors. Although some light sources surpass the work function's energy, their low energy restricts the measurable momentum space severely. A recent breakthrough in a light source with a photon energy of 10.9 eV has overcome this limitation, ushering in the ToF option for photoelectron spectroscopy in modern laboratory systems [4].

Photoemission electron microscopy (PEEM) is a widely utilized technique for investigating electronic and magnetic properties on solid surfaces, encompassing tasks such as imaging magnetic domains [5–7], measuring work functions [8], and studying ultra-fast carrier dynamics in semiconductors [9]. Despite lacking energy analysis capability, PEEM boasts high spatial resolution [10]. Integrating a ToF analyzer into a PEEM column (ToF-PEEM) introduces energy analysis to PEEM images with remarkable resolution [11], rendering ToF-PEEM a viable spectroscopic technique. Recent advancements include time-resolved photoemission spectroscopy [12, 13] and spin analysis using a multi-channel spin detector [14, 15].

This study unveils a ToF-PEEM spectrometer coupled with a 10.9-eV laser. This innovative spectrometer achieves highly efficient data acquisition with exceptional spatial resolution in photoemission microscopy. Moreover, the PEEM lens systems facilitate swift switching between real and

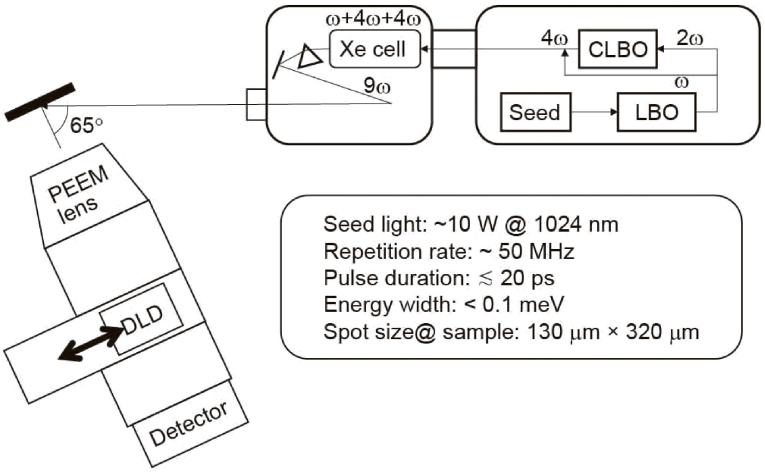

Figure 1: Schematic of ToF-PEEM and laser specifications.

momentum spaces. This functionality enables rapid identification of the region of interest in the sample's real space, followed by an examination of the band structure in the momentum space.

II. INSTRUMENT

A. Analyzer and light source

The ToF-PEEM consists of six components, as illustrated in Figure 1, with laser specifications detailed for the relevant parts [16]. The system operates in two modes for acquiring photoelectron images: the conventional PEEM measurement mode utilizing a multi-channel plate and a CMOS camera set, and the ToF mode employing a delay-line detector (DLD, Roentdek DLD40). In the conventional PEEM mode, an energy-integrated photoelectron image is obtained, while the ToF mode captures an energy-resolved image instantaneously. Consequently, a three-dimensional dataset is constructed by adding energy to two dimensions (x, y, or k_x, k_y) simultaneously. The ToF drift tube is 457 mm long.

The laser employed is a commercial 10.9-eV (113.8-nm) device (OXIDE UV-3), utilizing the 9th harmonic of the fundamental Yb fiber laser. The fundamental is transformed into the second harmonic ($2\omega = 512$ nm) by the first SHG crystal (LiB_3O_5). Subsequently, the second SHG crystal ($CsLiB_5O_{10}$) converts the second harmonic into a fourth harmonic ($4\omega = 256$ nm). The Xe gas cell combines the two harmonics and the fundamental to generate the 9th harmonic ($9\omega = 4\omega + 4\omega + 1\omega = 113.8$ nm). With a repetition frequency of 50 MHz, only 1 pulse out of 32 is utilized due to the inability of DLDs to keep up with 50 MHz. The pulse width is $\lesssim$20 ps. The typical output power of the laser is 5 μW, and the spot size, as per literature [16], measures approximately 130 μm × 320 μm, with a photon flux of 6.9×10^{13} photons s^{-1} mm^{-2}. The number of photons per pulse is 1.4×10^7 photons mm^{-2} $pulse^{-1}$. Despite the extended pulse width, spatial charging effects are mitigated due to the low photon density. The high photon flux per second enables extremely efficient measurements to be made. The energy width is less than 0.1 meV, ensuring suitability for high-resolution photoemission spectroscopy measurements. The light, horizontally, vertically, clockwise, and counterclockwise polarized, is focused onto the sample through a concave mirror at an irradiation angle of 65° from the sample surface normal direction. To prevent absorption by water and oxygen, the laser chamber is filled with argon gas and isolated from the ultrahigh vacuum by a LiF window.

B. Conversion from time to energy

Figure 2(a) presents a ToF-detector-captured PEEM image of a sample featuring silver pads deposited on a silicon substrate. The trench width between the silver pads measures 2 μm, with a period of 10 μm between the pads. The silver pad pattern is clearly discernible. The intensity profile along the x-direction within the yellow square in the figure is depicted in Figure 2(b). Fitting the result by convolving a step function with a Gaussian function reveals a full width at half maximum of 70 nm, indicative of a spatial resolution of at least 70 nm. This value is the upper limit of the spatial resolution in this system because it implies the edge steepness of the Ag pads. The ToF detector used for these images allows the determination of photoelectron kinetic energy from the delay time. The process involves capturing the time dependence of the photoelectron intensity (time spectrum), applying a bias voltage to the sample concerning the analyzer to shift the spectrum, and obtaining the full-time spectrum [Figure 2(c)]. The change in the time position of the peak due to this bias is linearly approximated, enabling the conversion of energy from the delay time. Figure 2(d) illustrates the dependence of the peak position on the bias voltage, demonstrating an almost linear relationship. Fitting with a straight line yields a slope of 1.375 ns V^{-1}. Given the system's smallest time step of 64 ps, the smallest energy step is approximately 50 meV. Notably, the time resolution of the ToF, rather than the electron lens system, currently dictates the energy resolution.

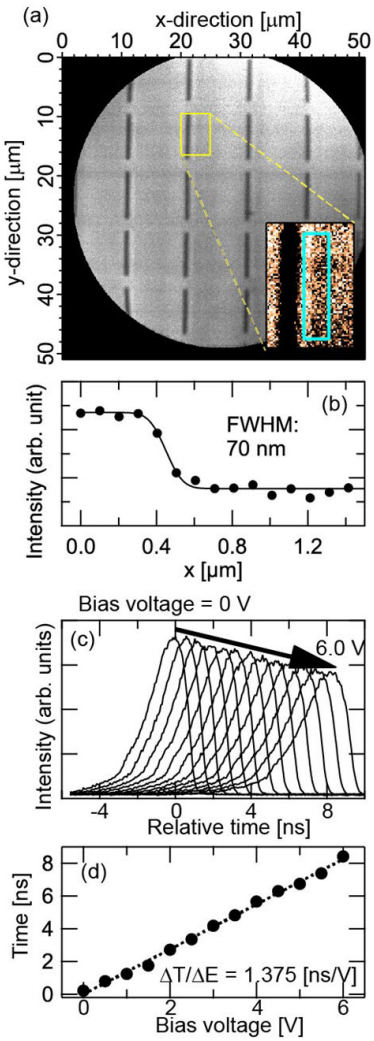

Figure 2: (a) Photoelectron intensity mapping of the square grid pattern of Ag on the Si substrate in real space with a field of view (FoV) of 50 μm. The inset is an enlarged image of the yellow box in the main panel. (b) Photoemission intensity profile along the *x*-direction inside the square in panel (a). (c) Spectral change due to bias application. (d) Relationship between energy and delay time.

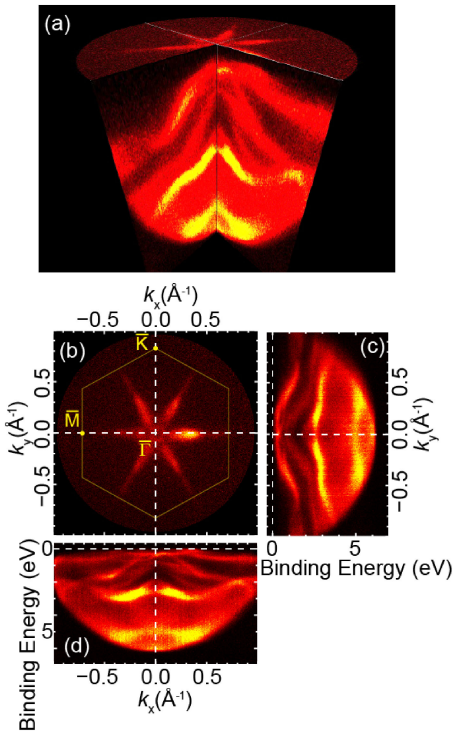

Figure 3: (a) ARPES intensity mapping of the Bi(111) film on the Ge(111) substrate in the E–k_x–k_y cube. (b) Photoemission intensity mapping in a k_x–k_y plane at the Fermi level. (c) Photoemission intensity mapping in an E–k_x plane at the $k_y = 0$ line. (d) Photoemission intensity mapping in an E–k_y plane at the $k_x = 0$ line. The surface Brillouin zone is superimposed by yellow thin lines on panel (b). The incident light plane is parallel to $\bar{\Gamma}\bar{M}$, and p-polarized light was used.

III. DEMONSTRATION

As an illustration of the ARPES measurement using the ToF-PEEM system, we performed ARPES on a Bi(111) single crystal film grown on a Ge(111) substrate. The clean surface of the substrate was achieved through several cycles of Ar^+ sputtering and annealing up to 600°C, confirmed by a sharp low-energy-electron-diffraction (LEED) pattern displaying $c(2 \times 8)$ periodicity [17]. Subsequently, a 100-nm Bi film was deposited at room temperature (RT) via molecular beam epitaxy and annealed at 400 K [18]. The deposition rate was monitored using a quartz microbalance, and orderliness of the Bi film was verified by a distinct (1×1) LEED pattern, consistent with prior research [18]. ARPES measurements were performed at RT.

Figure 3 presents k_x–k_y intensity mapping at the Fermi level [Figure 3(a)], an E–k_x map along the $\bar{\Gamma}\bar{M}$ direction [Figure 3(b)], and an E–k_y map along the $\bar{\Gamma}\bar{K}$ direction [Figure 3(d)]. These data were acquired within a real-space field of view of 50 μm. The energy range covered the entire observable spectrum from Fermi energy to kinetic energy 0. At the Fermi level, we observed a circular Fermi surface centered at the $\bar{\Gamma}$ point and six elliptical Fermi surfaces extending to the $\bar{\Gamma}\bar{M}$ direction, representing surface states of Bi(111), consistent with prior studies [19]. Additionally, several bands emerged on the deeper binding energy side, corresponding to bulk states and continuums [20]. As evident in Figure 3(b, c), the photoelectron intensity is observed within a parabola (the so-called photoelectron horizon) with a bottom at $E_B = 6.2$ eV, aligning with previous studies [20]. This example illustrates that a 10.9-eV laser facilitates measurements across a broad range in both momentum space and energy direction. In the case of the Bi(111) film, the Fermi surfaces of the entire Brillouin zone and a band a few eV near the Fermi level could be observed [16].

The acquisition time for the full band mapping depicted in Figure 3 was only 20 min, allowing for swift data acquisition from numerous measurement points. Furthermore, the ToF-PEEM spectrometer can be also utilized to measure the samples before contaminated.

IV. SUMMARY

In summary, we constructed a ToF-PEEM using a 10.9-eV laser, achieving a spatial resolution of 70 nm in real space. Additionally, we established an energy calibration method and successfully conducted microscopic ARPES measurements on a Bi film on a Ge substrate, obtaining data across all measurable regions in just 20 min.

Acknowledgments

The authors thank Nils Weber for technical support in developing the spectrometer. The present work was partially supported by the Japan Society for the Promotion of Science KAKENHI (Grant Nos. JP21K04633 and JP22H01761), the Innovative Science and Technology Initiative for Security Grant Number JPJ004596, ATLA, Japan, and Iketani Science and Technology Foundation.

References

[1] S. Hüfner, *Photoelectron Spectroscopy: Principles and Applications* (Springer-Verlag, Berlin, Heidelberg, 2003).
[2] T. Shimojima, K. Okazaki, and S. Shin, J. Phys. Soc. Jpn. **84**, 072001 (2015).
[3] R. Z. Bachrach, F. C. Brown, and S. B. M. Hagström, J. Vac. Sci. Technol. **12**, 309 (1975).
[4] Y. He, I. M. Vishik, M. Yi, S. Yang, Z. Liu, J. J. Lee, S. Chen, S. N. Rebec, D. Leuenberger, A. Zong, C. M. Jefferson, R. G. Moore, P. S. Kirchmann, A. J. Merriam, and Z.-X. Shen, Rev. Sci. Instrum. **87**, 011301 (2016).
[5] T. Nakagawa, T. Yokoyama, M. Hosaka, and M. Katoh, Rev. Sci. Instrum. **78**, 023907 (2007).
[6] J. Vogel, W. Kuch, M. Bonfim, J. Camarero, Y. Pennec, F. Offi, K. Fukumoto, J. Kirschner, A. Fontaine, and S. Pizzini, Appl. Phys. Lett. **82**, 2299 (2003).
[7] M. Kotsugi, C. Mitsumata, H. Maruyama, T. Wakita, T. Taniuchi, K. Ono, M. Suzuki, N. Kawamura, N. Ishimatsu, M. Oshima, Y. Watanabe, and M. Taniguchi, Appl. Phys. Express **3**, 013001 (2010).
[8] W. Y. Li, K. Goto, and R. Shimizu, Surf. Interface Anal. **37**, 244 (2005).
[9] K. Fukumoto, K. Onda, Y. Yamada, T. Matsuki, T. Mukuta, S. Tanaka, and S. Koshihara, Rev. Sci. Instrum. **85**, 083705 (2014).
[10] T. Taniuchi, Y. Kotani, and S. Shin, Rev. Sci. Instrum. **86**, 023701 (2015).
[11] H. Spiecker, O. Schmidt, C. Ziethen, D. Menke, U. Kleineberg, R. C. Ahuja, M. Merkel, U. Heinzmann, and G. Schönhense, Nucl. Instrum. Methods Phys. Res. A **406**, 499 (1998).
[12] J. Madéo, M. K. L. Man, C. Sahoo, M. Campbell, V. Pareek, E. L. Wong, A. Al-Mahboob, N. S. Chan, A. Karmakar, B. M. K. Mariserla, X. Li, T. F. Heinz, T. Cao, and K. M. Dani, Science **370**, 1199 (2020).
[13] O. Karni, E. Barré, V. Pareek, J. D. Georgaras, M. K. L. Man, C. Sahoo, D. R. Bacon, X. Zhu, H. B. Ribeiro, A. L. O'Beirne, J. Hu, A. Al-Mahboob, M. M. M. Abdelrasoul, N. S. Chan, A. Karmakar, A. J. Winchester, B. Kim, K. Watanabe, T. Taniguchi, K. Barmak, J. Madéo, F. H. da Jornada, T. F. Heinz, and K. M. Dani, Nature **603**, 247 (2022).
[14] G. Schönhense, K. Medjanik, S. Chernov, D. Kutnyakhov, O. Fedchenko, M. Ellguth, D. Vasilyev, A. Zaporozhchenko-Zymakoová, D. Panzer, A. Oelsner, C. Tusche, B. Schönhense, J. Braun, J. Minár, H. Ebert, J. Viefhaus, W. Wurth, and H. J. Elmers, Ultramicroscopy **183**, 19 (2017).
[15] D. Kutnyakhov, S. Chernov, K. Medjanik, R. Wallauer, C. Tusche, M. Ellguth, S. A. Nepijko, M. Krivenkov, J. Braun, S. Borek, J. Minár, H. Ebert, H. J. Elmers, and G. Schönhense, Sci. Rep. **6**, 29394 (2016).
[16] K. Yaji and S. Tsuda, e-J. Surf. Sci. Nanotechnol. **22**, 46 (2024).
[17] I. Razado-Colambo, J. He, H. M. Zhang, G. V. Hansson, and R. I. G. Uhrberg, Phys. Rev. B **79**, 205410 (2009).
[18] S. Hatta, Y. Ohtsubo, S. Miyamoto, H. Okuyama, and T. Aruga, Appl. Surf. Sci. **256**, 1252 (2009).
[19] T. Hirahara, T. Nagao, I. Matsuda, G. Bihlmayer, E. V. Chulkov, Y. M. Koroteev, P. M. Echenique, M. Saito, and S. Hasegawa, Phys. Rev. Lett. **97**, 146803 (2006).
[20] A. Kimura, E. E. Krasovskii, R. Nishimura, K. Miyamoto, T. Kadono, K. Kanomaru, E. V. Chulkov, G. Bihlmayer, K. Shimada, H. Namatame, and M. Taniguchi, Phys. Rev. Lett. **105**, 076804 (2010).